Measurement and modelling of magnetic properties of soft magnetic composite material under 2D vector magnetisations

Y.G. Guo*, J.G. Zhu, and J.J. Zhong

Faculty of Engineering, University of Technology, Sydney, P.O. Box 123, Broadyway, NSW 2007, Australia

* Corresponding author: Tel: +61-2-95147903, Fax: +61-2-95142435, E-mail: youguang@eng.uts.edu.au

Abstract

This paper reports the measurement and modelling of magnetic properties of SOMALOY^{TM} 500, a soft magnetic composite (SMC) material, under different 2D vector magnetisations, such as alternating along one direction, circularly and elliptically rotating in a 2D plane. By using a 2D magnetic property tester, the B-H curves and core losses of the SMC material have been measured with different flux density patterns on a single sheet square sample. The measurements can provide useful information for modelling of the magnetic properties, such as core losses. The core loss models have been successfully applied in the design of rotating electrical machines with SMC core.

PACS: 75.50.Gg

Keywords: 2D magnetic property; 2D Vector Magnetisation; Soft magnetic composite; Magnetic Measurement; Magnetic Modelling.

1. Introduction

Soft magnetic composite (SMC) materials and their application in electromagnetic devices have been a strong interest of research in the past decade due to their unique properties, such as magnetic and thermal isotropy, extremely low eddy current loss and relatively low total core loss at medium and higher frequencies, nearly net-shape fabrication process (no need of further machining), and the prospect of very low cost mass production [1]. The basis for the material is the bonded iron powder of high purity and high compressibility. The powder particles are bonded with a coating of high electrical resistivity. The coated powder is then pressed into a solid material using a die and finally heat treated to anneal and cure the bond.

This type of material is in general magnetically isotropic due to its powdered nature and this creates key design benefits for electromagnetic devices. The magnetic circuits can now be designed with three-dimensional (3D) flux path and radical topologies can be exploited to achieve high machine performance because the magnetic field does not have to be constrained in a plane as that in laminated steels, which are commonly used in rotating electrical machines and transformers [2]. Typical examples of SMC application are claw pole and transverse flux machines, in which the magnetic field is really three-dimensional due to the complex structure of the machines [3].

In electrical machines with 3D flux, the **B** (flux density) locus at one location can be very complicated when the rotor rotates, such as one-dimensional (1D) alternating, two-dimensional (2D) or even 3D circularly or elliptically rotating, all with or without harmonics [4]. Therefore, the magnetic properties of the magnetic material under various vector magnetisations should be investigated and properly considered in the design and analysis of

3D flux machines. However, the only available data, provided by the manufacturer, was obtained by the 1D alternating measurements with a standard ring sample [5]. This paper summarises our work about the magnetic measurement and modelling of SOMALOY^{TM} 500 under different vector magnetisations, and the application of the modelling in SMC motor design.

2. 2D Magnetic Testing System

Since the rotational magnetic properties such as rotational power losses in electrical sheet steels were quantitatively measured for the first time by Baily in 1896 [6], a large number of measuring techniques and testing systems have been developed for rotational measurement. Among these testers, the square sample single sheet tester (SST) initiated by Brix *et al.* [7] appears to be the most favourable, because it is more flexible to control the rotating magnetic flux pattern and the magnetic field in the sample is more uniform and hence the measurement accuracy is higher.

A single sheet tester for square specimen, developed at the University of Technology, Sydney (UTS) in 1993 [8] and modified in 1997, was used for the measurement of the magnetic properties of SMC materials under 2D magnetic excitations. Fig. 1 illustrates schematically the square sample SST and the whole testing system.

The 2D magnetic field in the sample is generated by two groups of excitation coils arranged on the X- and Y-axes, respectively. The excitation voltages and currents are supplied by two identical power amplifiers. By controlling the waveforms, magnitudes and phase angles of the excitation voltages on the two axes, any complex 1D or 2D magnetic flux density vector, such as an alternating magnetic flux density inclined at a specified angle from the X- or Y-axis, a

purely circular or elliptical rotating magnetic flux density, or a rotating magnetic flux density of any specified locus, can be generated. For the feedback control of the magnetic flux density components on the X- and Y-axes, two specially designed differential amplifiers with low and high pass filters are employed. A PC based digital signal processing system is used for both function generation and data acquisition.

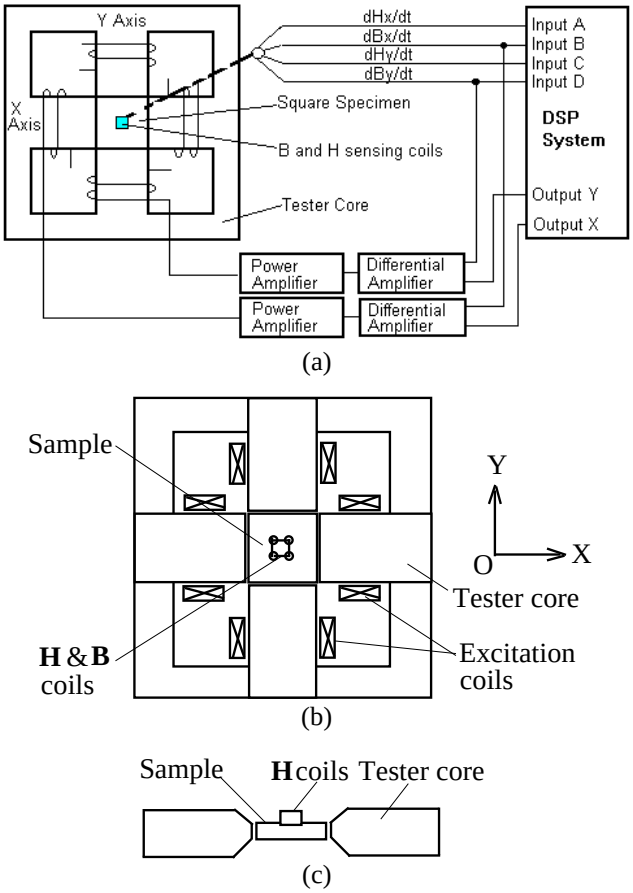

Fig. 1. Schematic illustration of (a) block diagram of the 2D magnetic testing system, (b) the square specimen SST, and (c) position of the sample between the magnetisation poles.

To determine the total core loss and **B**-**H** relationship in the sample, the flux density **B** inside the sample and the field strength **H** on the surface should be measured accurately. In this testing, 2D Rogowski-Chattock H-coils are employed for the measurement of the surface

field strength. The coils are installed very close to the sample surface to pick up the correct value of the surface field strength. B-coils are used for the measurement of the flux density because of their high accuracy. For measuring the rotational core loss, the field-metric method was employed, featuring high accuracy and great versatility. Moreover, the measured instantaneous **H** and **B** values can yield additional information, such as various loss contributions, the loci of **H** and **B** vectors, and harmonics, etc. By the Poynting's theorem, the total core loss P_t in the samples can be obtained by

$$P_t = \frac{1}{T\rho_m}\int_0^T \mathbf{H} \bullet \frac{d\mathbf{B}}{dt} dt = \frac{1}{T\rho_m}\int_0^T (H_x \frac{dB_x}{dt} + H_y \frac{dB_y}{dt}) dt \quad (1)$$

where T is the time period of one magnetisation process, ρ_m the sample mass density, and H_x, H_y, B_x and B_y are the X- and Y-components of **H** and **B**, respectively.

3. 2D Magnetic Measurements

The SMC sample of 50 mm × 50 mm × 1.25 mm, was cut from a cylindrical SOMALOY^{TM} 500 preform of 80 mm in diameter and 50 mm in height. The sample has been systematically tested under various alternating **B** vectors at both the X- and Y-axes, and circular and elliptical **B** vectors as well in both the clockwise and anti-clockwise directions, at 5 Hz, 10 Hz, 20 Hz, 30 Hz, 40 Hz, 50 Hz and 100 Hz, respectively.

Fig. 2 shows the B-H loops of the sample under 50 Hz sinusoidal excitations on the X- and Y-axes, respectively. The difference between the B-H loops on the two axes is quite small, implying that the material is almost isotropic.

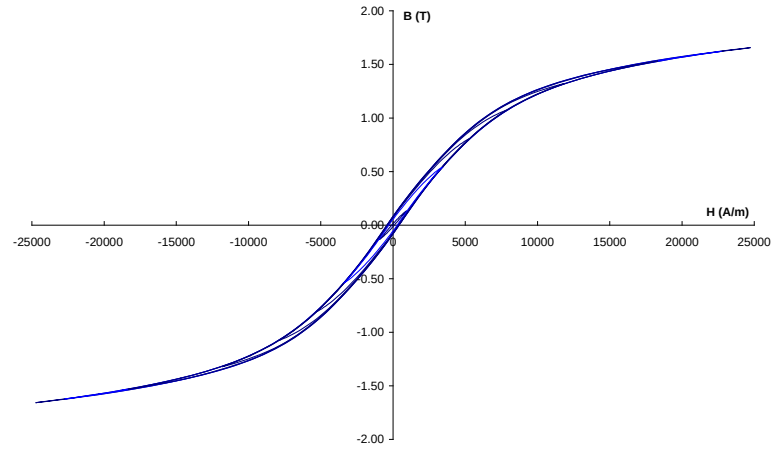

(a)

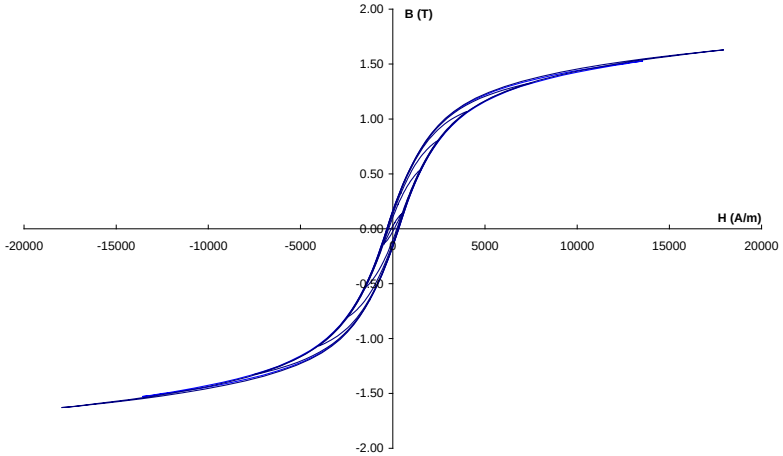

(b)

Fig. 2. B-H loops of SMC sample under 50Hz sinusoidal **B** vectors on (a) the X-axis, and (b) the Y-axis.

Fig. 3 plots the **B** and **H** loci with circular rotating **B** vectors at 50 Hz. It can be seen that when the **B** locus is controlled as circular, the corresponding **H** locus is elliptical (with harmonics) and its major and minor axes deviate from the coordinate ones. This implies that **B** and **H** vectors do not lie in the same direction and the ratio of their magnitudes varies with time.

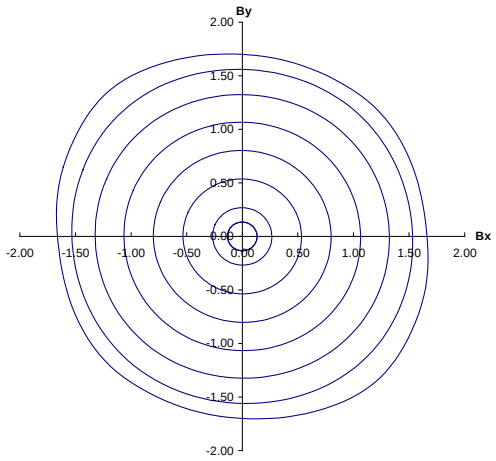

(a)

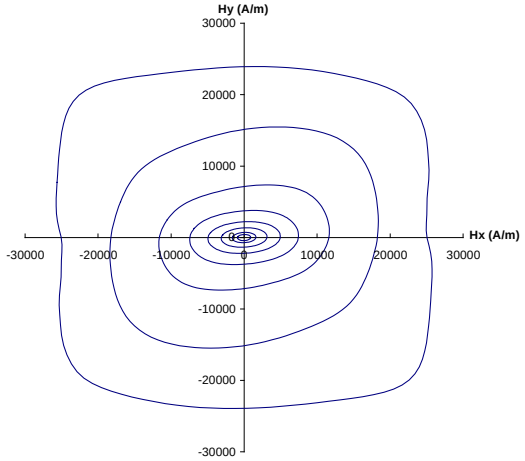

(b)

Fig. 3. Loci of **B** and **H** under 50 Hz circular **B** vectors

The core losses can be determined from the measured B_x, B_y, H_x and H_y by using (1). Fig. 4 shows the alternating and purely rotational core losses with different frequencies and peak flux densities. The rotational core losses have been corrected by using both the rotational coordinate transformation and the averaging method to minimize the measurement error caused by the misalignment of the sensing coils [9]. The alternating curves are obtained by averaging the measured alternating core losses on the X-axis and Y-axis, and the rotating curves are the average of the measurements along the clockwise and anticlockwise directions.

It is noticeable from Fig. 4 that the rotational core loss behaves very differently from its alternating counterpart. A rotational field causes nearly twice the loss produced by an alternating field with the same peak value at a mid-range flux density, but at the saturation level the loss caused by a rotating field falls markedly to the levels well below that caused by an alternating field. Therefore, it is necessary to have proper formulations for different types of core losses.

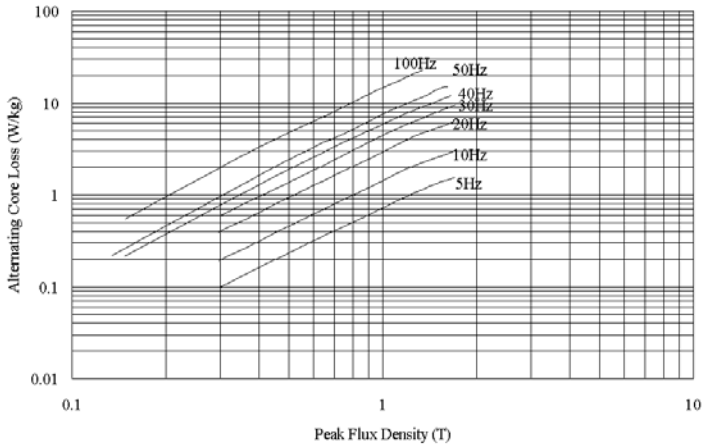

(a)

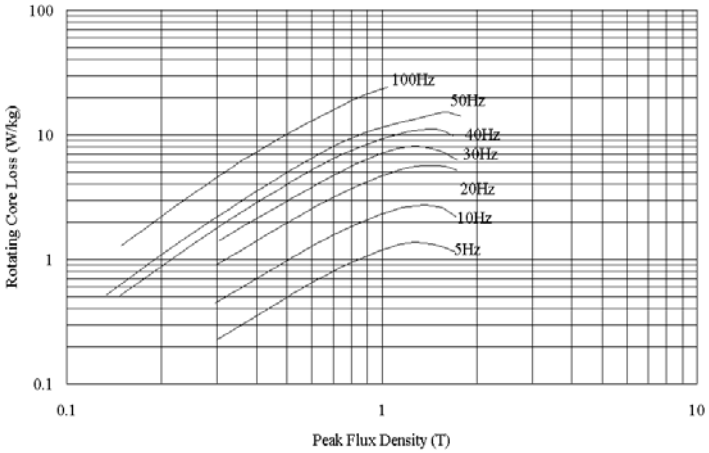

(b)

Fig. 4. Core losses under (a) alternating & (b) circular **B** vectors at different frequencies and magnitudes

4. Core Loss Models in SMC Samples

For the calculation of the alternating core loss, the three-term model is commonly used. The total loss is separated into three terms: hysteresis, eddy current and anomalous losses, as

$$P_a = C_{ha} fB_P{}^h + C_{ea}(fB_P)^2 + C_{aa}(fB_P)^{1.5} \quad (2)$$

where B_P is the peak value of flux density, f the frequency, and C_{ha}, h, C_{ea} and C_{aa} are the coefficients for hysteresis, eddy current and anomalous losses, respectively. By fitting (2) to the measured data in Fig. 4(a), these constants are deduced as C_{ha}=0.1402, h=1.548, C_{ea}=1.233x10^{-5}, and C_{aa}=3.645x10^{-4}. It is shown that the eddy current and anomalous losses are negligible within the low frequency range, comparing with the hysteresis loss. At 100 Hz, the eddy current loss and anomalous losses are only 0.1% and 2.6% of the hysteresis loss.

The specific circular core loss is also separated into three terms, i.e. rotational hysteresis, rotational eddy current and rotational anomalous losses, as

$$P_r = P_{hr} + C_{er}(fB_P)^2 + C_{ar}(fB_P)^{1.5} \quad (3)$$

where P_{hr} is the rotational hysteresis loss and C_{er} and C_{ar} are the coefficients for the rotational eddy current and anomalous losses, respectively. The ratio of rotational hysteresis loss to alternating hysteresis loss at low to middle range of flux density varies from 1 to 2 for different materials as reported by different researchers. At the saturation level, however, the hysteresis loss caused by a rotating field falls quickly, whereas the alternating hysteresis loss continues to increase.

To model the rotational hysteresis loss, a formulation was proposed in [10]. It is postulated that the specific rotational hysteresis loss per cycle can be expressed in terms of four

parameters, a_1 [in J/kg], a_2 [non-dimensional], a_3 [non-dimensional], and B_s [in T] as the following:

$$\frac{P_{hr}}{f} = a_1\left[\frac{1/s}{(a_2+1/s)^2+a_3^2} - \frac{1/(2-s)}{[a_2+1/(2-s)]^2+a_3^2}\right] \tag{4}$$

where

$$s = 1 - \frac{B}{B_s}\sqrt{1-\frac{1}{a_2^2+a_3^2}} \tag{5}$$

By fitting the formulations to the measured data in Fig. 4(b), the coefficients for the tested SMC sample are obtained as C_{er}= 2.303x10^{-4}, C_{ar}= 0, a_1= 6.814, a_2= 1.054, a_3= 1.445, and B_s= 2.134.

5. Flux Density Loci in SMC Motors with 3D Flux

Because in 3D flux machines the magnetic field distribution is very complex, 3D FEA is necessary for accurate determination of the flux density loci inside the machines. The locus of the flux density vector in each finite element can be obtained by a series of field solutions when the rotor rotates. The corresponding core loss dissipated in the element can then be calculated according to the locus of the flux density vector in the element.

As an example, Fig. 5 illustrates the flux density locus in a typical element in the middle of the claw pole of a three-phase three stack PM claw pole motor with SMC stator core [11]. It is noticed that the flux density vector has significant component along any coordinate axis, and rotates elliptically.

The three-phase motor has an inner SMC stator with 3 stacks and 3 coils, and an outside rotor with an array of 20 NdFeB magnets for each phase, mounted on the inner surface of the

mild steel rotor yoke. The major dimensions include the outer diameter of 94 mm, effective axial length of 93 mm, stator outer diameter of 80 mm, and main airgap length of 1 mm. The motor has successfully operated with a sensorless brushless DC controller, delivering an output power of 500 W at 1800 rev/min.

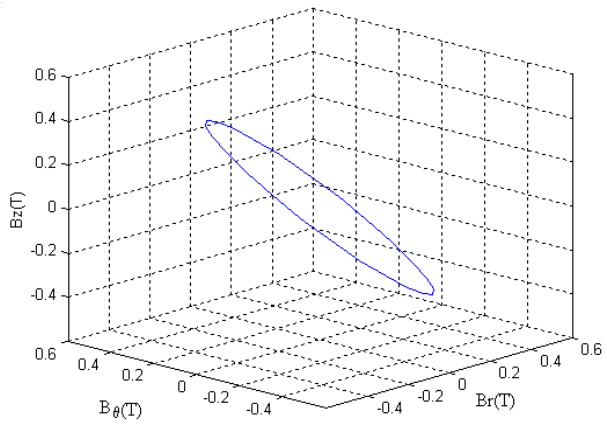

Fig. 5. No-load flux density locus in a typical element in the claw pole of a PM claw pole SMC motor

6. Models of Core Losses in 3D Flux SMC Motors

For any pattern of **B** locus in an element, its three components can always be expanded into Fourier series:

$$B_r(t) = \sum_{k=0}^{\infty}[B_{rsk}\sin(2\pi kft) + B_{rck}\cos(2\pi kft)] = \sum_{k=0}^{\infty} B_{rmk}\sin(2\pi kft + \phi_{rk}) \quad (6a)$$

$$B_\theta(t) = \sum_{k=0}^{\infty}[B_{\theta sk}\sin(2\pi kft) + B_{\theta ck}\cos(2\pi kft)] = \sum_{k=0}^{\infty} B_{\theta mk}\sin(2\pi kft + \phi_{\theta k}) \quad (6b)$$

$$B_z(t) = \sum_{k=0}^{\infty}[B_{zsk}\sin(2\pi kft) + B_{zck}\cos(2\pi kft)] = \sum_{k=0}^{\infty} B_{zmk}\sin(2\pi kft + \phi_{zk}) \quad (6c)$$

where B_r, B_θ and B_z are the radial, circumferential and axial components of the rotating flux density; B_{rmk}, $B_{\theta mk}$ and B_{zmk} are the magnitudes of the k-th harmonics of B_r, B_θ and B_z; and ϕ_{rk}, $\phi_{\theta k}$ and ϕ_{zk} are the phase angles of these harmonics, respectively, and t is the time.

Any order harmonic of these three components will form an elliptical trajectory in a plane, which may not be parallel to any coordinate axis. The two axes can be calculated by

$$B_{msk} = \sqrt{B_{rsk}^{\ 2} + B_{\theta sk}^{\ 2} + B_{zsk}^{\ 2}} \tag{7a}$$

$$B_{mck} = \sqrt{B_{rck}^{\ 2} + B_{\theta ck}^{\ 2} + B_{zck}^{\ 2}} \tag{7b}$$

The larger of B_{msk} and B_{mck} is taken as the major axis B_{kmaj} and the other as the minor axis B_{kmin} of the k-th harmonic of the elliptical flux density vector.

For the elliptical **B** vector of any order harmonic, the core loss can be predicted using the alternating formulations (2) and purely circular ones (3-5) by [10]

$$P_t = R_B P_r + (1 - R_B)^2 P_a \tag{8}$$

where R_B=B_{min}/B_{maj} is the axis ratio of $\boldsymbol{B}$, B_{maj} and B_{min} are the major and minor axes of the elliptical $\boldsymbol{B}$ locus, P_r and P_a are the core losses under a circular $\boldsymbol{B}$ with B_{maj}= B_{min}=B_p, and an alternating $\boldsymbol{B}$ with B_{maj}=B_p, respectively, and B_p the peak value of the alternating $\boldsymbol{B}$.

The core loss in an element can be obtained by summing up the contributions from all the flux density harmonics. Therefore, the total loss is

$$P_t = \sum_{k=0}^{\infty} \left[P_{rk} R_{BK} + (1 - R_{BK})^2 P_{ak} \right] \tag{9}$$

where R_{BK}=B_{kmin}/B_{kmaj} is the axis ratio of the k-th harmonic flux density, P_{rk} is the circularly rotational loss determined by (3), and P_{ak} is the alternating loss determined by (2).

7. Core Loss Computation of a Claw Pole Motor

The above formulations have been successfully applied to predict the core losses in PM claw pole SMC motors [4, 11]. Fig. 6 shows the computed core losses of the three-phase three stack PM claw pole motor with SMC stator core at no-load [11]. To validate the core loss models and computation, the core losses are measured by the "dummy stator method". The theoretical calculations agree with the measurements on the prototype.

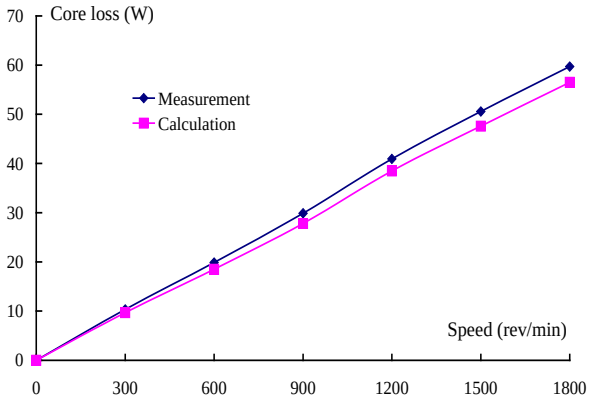

Fig. 6. Computed and measured no-load core losses of a three phase PM claw pole SMC motor

5. Conclusion

The magnetic properties of an SMC material, SOMALOY^{TM} 500, have been systematically measured under various 2D **B** vector magnetisations with different frequencies and different peak values, and the measurements can be used to derive the coefficients of core loss models. Different formulations are applied for the computation of core losses under alternating, circularly rotating and elliptically rotating **B** loci, respectively. As an example, the core losses of two claw pole SMC motors have been satisfactorily computed by using the formulations, in combination with 3D magnetic field FEA and Fourier series analysis.

Reference:

[1] "The latest development in soft magnetic composite technology", Reports of Höganäs AB, Sweden, 1997-2005. Available at http://www.hoganas.com, see News then SMC update.

[2] A.G. Jack, "Experience with the use of soft magnetic composites in electrical machines", in Proc. Int. Conf. on Electrical Machines, Istanbul, Turkey, 1998, pp1441-1448.

[3] Y.G. Guo, J.G. Zhu, P.A. Watterson, and W. Wu, "Comparative study of 3-D flux electrical machines with soft magnetic composite core", IEEE Trans. Industry Applications, Vol.39, Nov./Dec. 2003, pp1696-1703.

[4] Y.G. Guo, J.G. Zhu, J.J. Zhong, and W. Wu, "Core losses in claw pole permanent magnet machines with soft magnetic composite stators", IEEE Trans. Magn., Vol.39, No.5, Sept. 2003, pp3199-3201.

[5] "Soft magnetic composites from Höganäs metal powders - SOMALOY™ 500", Höganäs Product Manual, 1997.

[6] F.G. Baily, "The hysteresis of iron and steel in a rotating magnetic field", Phil. Trans. Royal Soc. A, 1896, pp715-746.

[7] W. Brix, K.A. Hempel, and W. Schroeder, "Method for the measurement of rotational power loss and related properties in electrical steel sheets", IEEE Trans. Magn., Vol.18, No.6, Nov. 1982, pp1469-1471.

[8] J.G. Zhu and V.S. Ramsden, "Two dimensional measurement of magnetic field and core loss using square specimen tester", IEEE Trans. Magn., Vol.29, Nov. 1993, pp2995-2997.

[9] J.J. Zhong, Y.G. Guo, J.G. Zhu, and Z.W. Lin, "Characteristics of soft magnetic composite material under rotating fluxes", accepted for publication in J. Magnetism and Magnetic Materials. In press.

[10] J.G. Zhu and V.S. Ramsden, "Improved formulations for rotating core losses in rotating electrical machines", IEEE Trans. Magn., Vol.34, No.4, July 1998, pp2234-2242.

[11] Y.G. Guo, J.G. Zhu, P.A. Watterson, and W. Wu, "Development of a claw pole permanent magnet motor with soft magnetic composite stator", Australian J. Electrical & Electronic Eng., Vol.2, No.1, 2005, pp21-30.